Article

Efficient Quantification of Lipid Packing Defect Sensing by Amphipathic Peptides: Comparing Martini 2 and 3 with CHARMM36

Niek van Hilten, Kai Steffen Stroh, and Herre Jelger Risselada*

ACCESS | Metrics & More | Article Recommendations | SI Supporting Information

ABSTRACT: In biological systems, proteins can be attracted to curved or stretched regions of lipid bilayers by sensing hydrophobic defects in the lipid packing on the membrane surface. Here, we present an efficient end-state free energy calculation method to quantify such sensing in molecular dynamics simulations. We illustrate that lipid packing defect sensing can be defined as the difference in mechanical work required to stretch a membrane with and without a peptide bound to the surface. We also demonstrate that a peptide's ability to concurrently induce excess leaflet area (tension) and elastic softening—a property we call the "characteristic area of sensing" (CHAOS)—and lipid packing sensing behavior are in fact two sides of the same coin. In essence, defect sensing displays a peptide's propensity to generate tension. The here-proposed mechanical pathway is equally accurate yet, computationally, about 40 times less costly than the commonly used alchemical pathway (thermodynamic integration), allowing for more feasible free energy calculations in atomistic simulations. This enabled us to directly compare the Martini 2 and 3 coarse-grained and the CHARMM36 atomistic force fields in terms of relative binding free energies for six representative peptides including the curvature sensor ALPS and two antiviral amphipathic helices (AH). We observed that Martini 3 qualitatively reproduces experimental trends while producing substantially lower (relative) binding free energies and shallower membrane insertion depths compared to atomistic simulations. In contrast, Martini 2 tends to overestimate (relative) binding free energies. Finally, we offer a glimpse into how our end-state-based free energy method can enable the inverse design of optimal lipid packing defect sensing peptides when used in conjunction with our recently developed evolutionary molecular dynamics (Evo-MD) method. We argue that these optimized defect sensors—aside from their biomedical and biophysical relevance—can provide valuable targets for the development of lipid force fields.
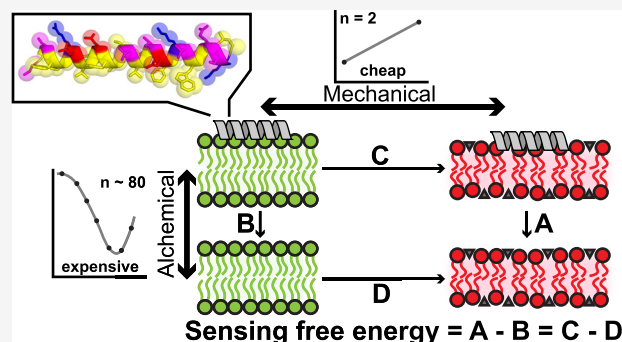
1. INTRODUCTION

Lipid bilayers are crucial for maintaining cellular integrity, structure, and homeostasis. Many processes taking place in, on, or near these membranes involve proteins that experience a thermodynamic force that drives the self-organization and recruitment toward certain bilayer properties such as curvature, tension, or lipid composition.[1−4] This process is called "sensing". A key feature that underlies such sensing is lipid packing defects that occur when membranes are stretched or bent. Regardless of whether this happens symmetrically (i.e., both leaflets experience the same tension) or asymmetrically (i.e., one leaflet gets stretched more than the other, resulting in a net positive curvature), the optimal packing of the hydrophilic lipid head groups gets disturbed, which exposes hydrophobic defects on the membrane surface. Due to the surfactant-like nature of amphipathic peptides and protein motifs, these differences in surface hydrophobicity can give rise to a difference in the relative binding free energy (membrane partitioning) and a concomitant sensing force.[5,6]

Many questions related to lipid packing defects can be challenging to address in experiments because these methods lack the required molecular detail. Hence, molecular dynamics (MD) simulations are an indispensable tool to study such membrane properties and their effect on protein binding and sensing. The crucial issue of the reliability of simulations is the quality of the force field, and many efforts, especially in the last several years, have been devoted to parametrization and optimization of the force fields for biomembrane modeling. For example, so-called "bottom-up" coarse-grained (CG) models, such as the Martini force field, are parametrized in a systematic way based on the reproduction of partitioning free energies between polar and apolar phases of a large number of chemical compounds.[7,8] A main goal of both atomistic and CG lipid force fields particularly is to accurately reproduce the
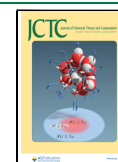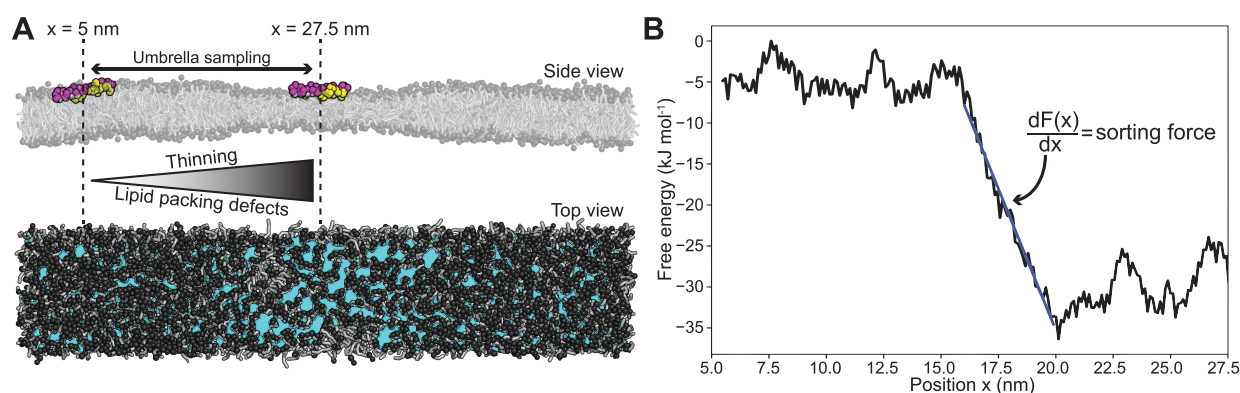
Figure 1. Qauntification of lipid packing defect sensing using the thermodynamic gradient method. Adapted from our previous work.[13] (A) Side view and top view of a flat Martini POPC membrane subject to an external potential that induces tension (thinning) in the middle section ($x = 27.5$ nm, thickness ≈ 3 nm) and is gradually switched off moving outward (to $x = 5$ nm, thickness ≈ 4 nm). Peptide model is ALPS. Cyan patches in the top view indicate lipid packing defects.[14] (B) Free energy ($F(x)$) as a function of the position (x) on the membrane calculated by umbrella sampling for ALPS across the lipid packing defect gradient. The slope of this curve ($\frac{\mathrm{d}F(x)}{\mathrm{d}x}$) is a thermodynamic sorting force, which can be directly used as a measure for lipid packing sensing. Linear behavior is explained by the linear decrease in membrane thickness along the gradient. Owing to bulk incompressibilty and hookian membrane elasticity, this results in a linear gradient in the surface tension and surface free energy whose spatial derivative yields a constant sorting force along the gradient.

membrane binding and partitioning of peripheral membrane proteins. However, a systematic comparison of force fields on the relative binding free energies, i.e., quantification of membrane curvature and lipid packing defect sensing, of whole proteins or even peptides is computationally not tractable using the present alchemical approaches such as thermodynamic integration (TI)[9] and the Bennett acceptance ratio (BAR) method.[10] Furthermore, (un)binding of peptides is subject to large hysteresis, which complicates accurate estimation of binding free energies when using free energy calculation methods that rely on physical rather than alchemical reaction coordinates (e.g., umbrella sampling). Finally, a prevailing need exists to develop methods that enable efficient and accurate quantification of a peptide's ability to sense lipid packing defects because of important pharmaceutical applications such as the design of broad-spectrum antiviral peptides that selectively target the highly curved lipid envelope of clinically relevant viruses.[11]

We recently illustrated how relative binding free energies due to differences in membrane curvature[12] and lipid packing defects[13] can be quantified in CG molecular simulations via umbrella sampling. With these studies, we also showed that curvature and lipid packing defect sensing are in fact equivalent phenomena, implying that a protein's ability to sense positive membrane curvature can be alternatively inferred from its ability to sense packing defects. Lipid packing defect sensing can be efficiently quantified from the magnitude of a thermodynamic sorting force that acts on a surface binding peptide when it is positioned within a spatial gradient of lipid packing defects—a defect gradient (Figure 1A).[13] Since the sorting force is approximately constant over the whole gradient (slope in Figure 1B), its magnitude is directly proportional to the relative free energy of membrane binding. Therefore, sensing can be quantified by ensemble averaging over only a single simulation. This approach yields accurate results given that the spatial gradient zone is smeared out over ~10 nm or more. However, the method still features a slow convergence of the sorting force via ensemble averaging (multiple microseconds) due to the asymmetric nature of the gradient in combination with slow orientational and rotational modes of

the peptide when it is bound to the membrane. Furthermore, computational efficiency cannot be trivially improved via further reduction of the system size since too strong spatial gradients in membrane thickness also compromise the precision of the method. Thus, although the thermodynamic gradient method provides an elegant and intuitive method for quantifying lipid packing defect sensing, its slow convergence limits its application in high-throughput utilities and atomistic simulations.

Here, we present a highly efficient and accurate end-state free energy calculation method to directly estimate the relative free energy of membrane binding, i.e., quantification of defect and curvature sensing. In contrast to well-established *alchemical pathways*, we illustrate that the relative free energy of binding can be alternatively obtained using a *mechanical pathway*, which is equally accurate and computationally much less expensive. An important advantage of the new approach is that the corresponding end-state systems are both small (128 lipids) and symmetric, which enables quick and reliable calculation of the relative binding free energy in CG simulations and also makes them more feasible to conduct on the atomistic scale. We compare the performance and accuracy of this end-state mechanical pathway with the standard alchemical pathway (TI) by analyzing them for four known packing defect sensing peptides and two related negative controls. We also use this new quantification method to compare lipid packing defect sensing and overall peptide–membrane interactions within the recent Martini 3 force field[8] with the previous version and atomistic simulations.

Importantly, the here-resolved thermodynamic cycle illustrates that lipid packing sensing and the induction of membrane tension are in fact two sides of the same coin. This implies that defect sensing peptides maximize the generation of leaflet tension resulting in a strong native membrane destabilizing propensity. Finally, as the ultimate demonstration of the method's high-throughput potential, we will illustrate how our method can direct the simulated evolution of defect sensing peptides toward optimal sensing (inverse design). We argue that these optimal sequences provide novel and valuable benchmark systems since they
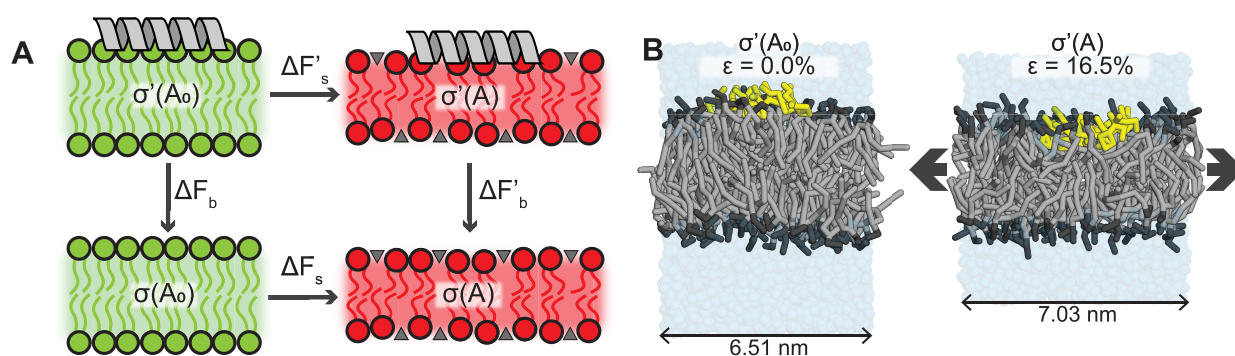
Figure 2. (A) Thermodynamic cycle that links the alchemical ($\Delta F_b' - \Delta F_b$) and the mechanical ($\Delta F_s' - \Delta F_s$) pathways. Tensionless and stretched membranes are shown in green and red, respectively. Lipid packing defects in the stretched membranes are depicted by the gray triangles. (B) Snapshots of the CG systems without tension (left, no relative strain ϵ) and with tension (right, high relative strain ϵ). POPC lipids are shown in gray with black head groups. Peptide is shown in yellow.

reflect the boundary of a force field's applicability domain. The primary aim of force fields is to reproduce physicochemical driving forces—trends, not just absolutes—and therefore, they must at least reproduce the global physicochemical features of optimized sequences.

2. THEORY AND METHODS

2.1. Alchemical Calculation of the Relative Binding Free Energy. Lipid packing defect sensing can be defined as the differential affinity of a peptide toward a membrane *with* defects ($\Delta F_b'$, under tension) versus a membrane *without* defects (ΔF_b, tensionless). Note that we use the nomenclature ΔF to indicate that the simulations were performed at a constant area (but not constant volume). In terms of free energy differences, we can write

$$\Delta\Delta F_{sensing} = \Delta F_b' - \Delta F_b \tag{1}$$

In membrane-binding experiments, the reference state for $\Delta F_b'$ and ΔF_b (membrane bound to unbound) is the peptide in solution, and besides a membrane partitioning term, it would also contain an energetic cost for (un)folding. However, we note that the solvation energy (water to vacuum) of a peptide is independent of the state of the membrane (under tension or tensionless), which causes these solvation terms to cancel out. In addition, switching off all peptide−system interactions renders its ensemble invariant to peptide folding events elsewhere in the thermodynamic cycle.

$\Delta F_b'$ and ΔF_b can be calculated using thermodynamic integration (TI).[9] In this commonly used "alchemical" method, a peptide−membrane bound state (A, with potential energy V_A) is transitioned to the peptide in vacuo (B, with potential energy V_B) by gradually switching off the van der Waals and Coulomb interactions between the peptide particles and their surroundings (coupling parameter $\lambda = 0 \rightarrow \lambda = 1$). By taking the integral of the ensemble average of the derivative of the potential energy ($V(\lambda)$), the free energy difference between states A and B can be calculated

$$\Delta F(A \rightarrow B) = \int_0^1 \left\langle \frac{\partial V(\lambda)}{\partial\lambda} \right\rangle_\lambda d\lambda$$
$$= \int_0^1 \langle V_B(\lambda) - V_A(\lambda)\rangle_\lambda d\lambda \tag{2}$$

Although TI is an accurate and commonly used method, it is—even when using CG force fields—computationally expensive.

To make sure the numerical integration is valid, a smooth $\frac{\partial V(\lambda)}{\partial\lambda}$ profile is required, which typically takes at least 20 λ states to simulate. Because decoupling is generally performed separately for the van der Waals and Coulomb interactions, the number of simulations increases to 30−40 per system. Moreover, in problems concerning the difference in binding free energies between two systems (like our packing defect sensing problem; $\Delta\Delta F_{sensing} = \Delta F_b' - \Delta F_b$), this again doubles to at least 60−80 simulations in total.

2.2. Mechanical calculation of the relative binding free energy. Consistent with the first law of thermodynamics, the energy difference between two states of a cycle is independent of the path one takes to get from one to the other. We can define such a cycle by connecting the two begin states (peptide bound) and the two end states of the alchemical pathway (peptide unbound); see Figure 2A. This realization allows a redefinition of lipid packing defect sensing as the change in work required to stretch a membrane in the presence ($\Delta F_s'$) and absence (ΔF_s) of a surface-bound peptide

$$\Delta\Delta F_{sensing} = \Delta F_b' - \Delta F_b = \Delta F_s' - \Delta F_s \tag{3}$$

Thus, a good lipid packing sensor ($\Delta\Delta F_{sensing} \ll 0$) minimizes the work required to stretch the membrane leaflet it adheres to.

Calculating this mechanical pathway is much cheaper compared to the alchemical pathway (TI) for two reasons. First, one of the terms, ΔF_s, is peptide independent, since it is simply the work required to stretch a membrane without a peptide bound to it. This means one only has to calculate it once (for a given system) and can simply plug in the same number for any peptide of interest. Second, in elastic theory, the lateral tension $\sigma(A)$ in a membrane is linearly related to the change in membrane area ($\frac{A - A_0}{A_0}$, i.e., relative leaflet strain ϵ) for small deviations from the equilibrium tensionless area A_0[15]

$$\sigma(A) = K_A\epsilon = K_A\frac{A - A_0}{A_0} \tag{4}$$

with K_A being the area compressibility modulus. The tension $\sigma(A)$ can be directly obtained via ensemble averaging at constant membrane area using the relation

$$\sigma(A) = \left(\frac{dF}{dA}\right)_A = L_z\left(P_z - \frac{1}{2}(P_x + P_y)\right) \tag{5}$$

where L_z is the length of the simulation box along the z dimension and P_x, P_y, and P_z are the average pressures in the x, y, and z dimensions, respectively. These pressures are derived from the diagonal components of the stress tensor as derived from the Clausius virial theorem.

Because of the linear relation in eq 4, the free energy difference (mechanical work) of stretching (ΔF_s) can be reliably approximated by performing MD simulations at merely two different constant areas A and A_0 and by measuring the resulting surface tensions $\sigma(A)$ and $\sigma(A_0)$. Applying the trapezoidal rule yields

$$\Delta F_s = \int_{A_0}^{A} \sigma(A)\mathrm{d}A = (A - A_0)\frac{\sigma(A) + \sigma(A_0)}{2} \quad (6)$$

This is where the biggest efficiency gain lies for the mechanical path (two points on a straight line) versus the alchemical path (integration over >20 points on a complicated $\frac{\partial V(\lambda)}{\partial \lambda}$ profile).

Now, combining and rearranging eqs 3 and 6 yields

$$\Delta\Delta F_{\text{sensing}} = \Delta F_s' - \Delta F_s = \int_{A_0}^{A} \sigma'(A)\mathrm{d}A - \int_{A_0}^{A} \sigma(A)\mathrm{d}A$$

$$= \frac{A - A_0}{2}[(\sigma'(A) + \sigma'(A_0)) - (\sigma(A) + \sigma(A_0))] \quad (7)$$

in which, like mentioned before, the membrane tensions in the peptide-free systems $\sigma(A)$ and $\sigma(A_0)$ only have to be measured once to be used in the calculations for any peptide.

2.3. System Setup. A simulation box containing 128 CG 16:0−18:1 phosphatidylcholine (POPC) lipids was generated using the *insane* python script.[16] After solvation with 1800 Martini water beads and a steepest descent minimization, the system was equilibrated with semiisotropic pressure coupling to obtain tensionless membrane conditions. Next, the area of the box was increased by steps of 1.4 nm^2 and reequilibrated every time (at constant area). 500 nanosecond production runs were performed for the resulting 6 membranes, the areas of which ranged from 42.4 to 49.4 nm^2 (Figure 2B). Such a 16.5% increase in leaflet area corresponds to the effective relative strain ($\epsilon = \frac{A - A_0}{A_0}$) in the outer leaflet of a $\sim$ 25 nm diameter vesicle (see SI), which is the lower size limit of vesicles found in nature.

Helical CG peptide models were generated using PeptideBuilder[17] in conjunction with martinize2−Ver-MoUTH[18] and placed 1.5 nm from the membrane center plane. For systems with charged peptides, counterions were added to neutralize the system. A steepest descent minimization with soft-core potentials (0.75 coupling for the van der Waals interactions) was performed to solve clashes. Production runs of 1−5 μs were performed, the first 50 ns of which were discarded from further analyses for equilibration.

For TI, the equilibrated setups for the minimal and maximal tension membranes were used as the starting points. 37 λ states were defined to ensure proper $\frac{\partial V(\lambda)}{\partial \lambda}$ sampling during separate decoupling of the van der Waals and Coulomb interactions (37 × 2 = 74) to the final in vacuo state. For the two setups—low and high tension—a total of 74 × 2 = 148 simulations of 500 ns was performed for each peptide. The Langevin stochastic dynamics (SD) integrator and thermostat were used for these runs. A soft harmonic distance constraint (k_{force} = 50 kJ mol^{-1} nm^{-2}) was used between the centers of mass of the membrane

and the peptide (z dimension only) to prevent peptide−membrane dissociation in high decoupling states. Finally, free energy differences were obtained through numerical integration (eq 2).

For buckled membrane simulations, initial configurations were generated with the python script *insane*.[16] Each membrane leaflet is comprised of 767 POPC lipids, which were put in the $x−y$ plane of a 40 nm × 10 nm × 20 nm simulation box. A curvature sensing peptide was placed close to the upper leaflet. The system was solvated with standard Martini water and a 0.15 M NaCl concentration. Following steepest-descent energy minimization and initial equilibration (50 ns NpT), the system was compressed in the x direction by applying a pressure of 3 bar (Berendsen barostat,[19] τ_p = 12.0 ps, compressibility of 3 × 10^{-4} bar^{-1}). The system was allowed to expand in the z direction, while the y dimension was fixed. From the compression trajectory, a frame close to a compression of 38% was chosen. Another NpT equilibration with fixed x and y dimensions (100 ns, Parrinello−Rahman barostat,[20] τ_p = 12.0 ps, compressibility of 3 × 10^{-4} bar^{-1}) followed. To fix the analytical shape of the buckled membrane, positions of the PO4 beads in the lower leaflet were restrained with a force constant of 10 kJ mol^{-1} nm^{-2}. This minimally influences the upper leaflet dynamics, where the peptide is located. For subsequent peptides the preequilibrated system was used, the original peptide was deleted, and a new peptide was inserted into the free volume. Energy minimization and NVT equilibration followed. To generate the initial configurations for the umbrella sampling, the peptide was pulled along the x direction of the membrane. Each individual umbrella sampling run is 1.05 μs long with the first 50 ns for equilibration. A harmonic potential with a force constant of k = 100 kJ mol^{-1} nm^{-2} was used to restrain the peptide to a defined point along the reaction coordinate. Rotation around the membrane normal was restrained in the same manner to keep the peptide aligned with the y axis, i.e., the flat direction of the membrane.

Atomistic POPC membranes were equilibrated at the same constant areas as in the CG simulations. Simulation boxes contained 4985 CHARMM TIP3P water molecules.[21,22] The helical atomistic peptide models were built by feeding the PeptideBuilder pdb files into CHARMM-GUI.[23] The resulting peptide structures were placed on the membranes following the same procedure as described for the CG simulations. Triplicate independent production runs of 1 μs were performed. The first 500 ns were not included in the analyses to allow for equilibration.

2.4. Simulation Details. All simulations were performed with GROMACS 2019.3[24] except for the simulations on a buckled membrane, which were done with GROMACS 2021.4. The temperature was kept at a constant 310 K by the velocity rescaling thermostat[25] (τ_T = 1 ps). Unless stated otherwise, simulations were performed with fixed x and y dimensions (constant area), i.e., Berendsen pressure coupling[19] was applied only in the z dimension (1 bar reference pressure with a 4.5 × 10^{-5} bar^{-1} compressibility).

Coarse-grained molecular dynamics (CGMD) simulations were performed with the Martini force field, version 3.0.0,[8] unless stated otherwise. A 30 fs time step was used for all CG simulations except the buckled membrane runs, which were performed with a 20 fs time step. van der Waals interactions were calculated with the shifted Verlet cutoff scheme,[26] and reaction-field electrostatics[27] describe the coulomb potentials,
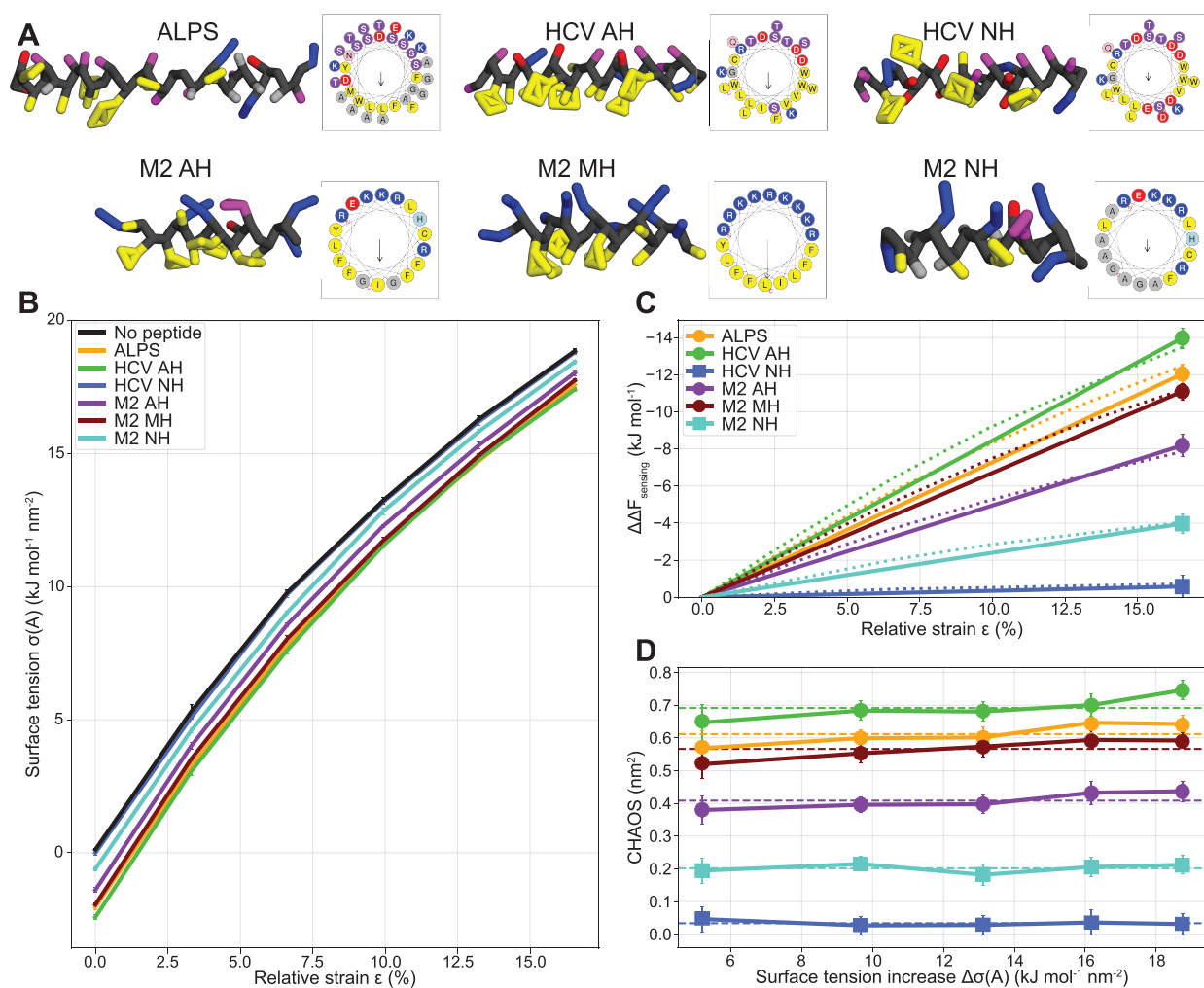
Figure 3. (A) Depictions of the helical peptide models in the Martini 3 model,[8] and full-sequence helical wheel representations.[43] Yellow: hydrophobic residues (C, F, I, L, M, V, W, Y). Red: negatively charged residues (D and E). Blue: positively charged residues (K and R). Magenta: polar residues (H, N, Q, S, and T). Gray: small residues (A and G) and backbone. (B) Surface tension measured at increasing membrane areas (relative strain $\epsilon = \frac{A - A_0}{A_0} \times 100\%$) with and without surface-bound peptides. (C) Sensing free energy differences at increasing relative strain, as calculated with eq 7, for different peptides. Dotted line represents the integral over all six points. Solid line represents the end-state method, which only integrates between the first ($\epsilon = 0\%$) and the last ($\epsilon = 16.5\%$) point. (D) Characteristic area of sensing (CHAOS parameter, see eq 8) is constant for different relative surface tension values ($\Delta\sigma(A) = \sigma(A_0) - \sigma(A)$), thereby illustrating its end-state-invariant nature. Dashed lines represent the average values for each peptide.

both with a 1.1 nm cutoff. The neighbor list was updated every 20 steps.

Atomistic simulations were done with the February 2021 version of the CHARMM36 force field.[22,28] A time step of 2 fs was used. van der Waals and Coulomb interactions were calculated using the Verlet scheme[26] (with forces switching off gradually between 1.0 and 1.2 nm) and the potential-shifted particle mesh Ewald (PME)[29] method, respectively, both with a 1.2 nm cutoff distance. The neighbor list was updated every 10 steps. The LINCS algorithm[30] was used to constrain bonds with hydrogen atoms.

3. RESULTS AND DISCUSSION

To demonstrate how our method works and to validate it against the well-established TI method, we will focus on the most broadly studied class of lipid packing sensing protein motifs: amphipathic α-helices. One side of these peptides mainly consists of large apolar/aromatic moieties to comple-

ment the hydrophobic lipid packing defects, and the other side comprises polar and/or positively charged residues to interact with the solvent and lipid headgroups. We picked six peptides for our study (Figure 3A), which we will briefly introduce below (see Table SI1 for details).

First, we will study the ALPS motif that allows curvature sensing by the ArfGAP1 protein[31] and is also found on other proteins.[32−35] Since its discovery, ALPS has served as an important model peptide in many computational studies on curvature/lipid packing sensing,[36−38] also in our own group.[12,13] Second, we will include an amphipathic helix (AH) that was derived from the NS5A protein of hepatitis C virus (HCV) and discovered to sense and rupture vesicles in a size-dependent manner: small vesicles (including HCV particles themselves) were more readily ruptured than bigger ones, and this size range overlaps with the diameter of many enveloped viruses (50−160 nm).[39,40] Indeed, the antiviral activity of HCV AH was later found for several unrelated
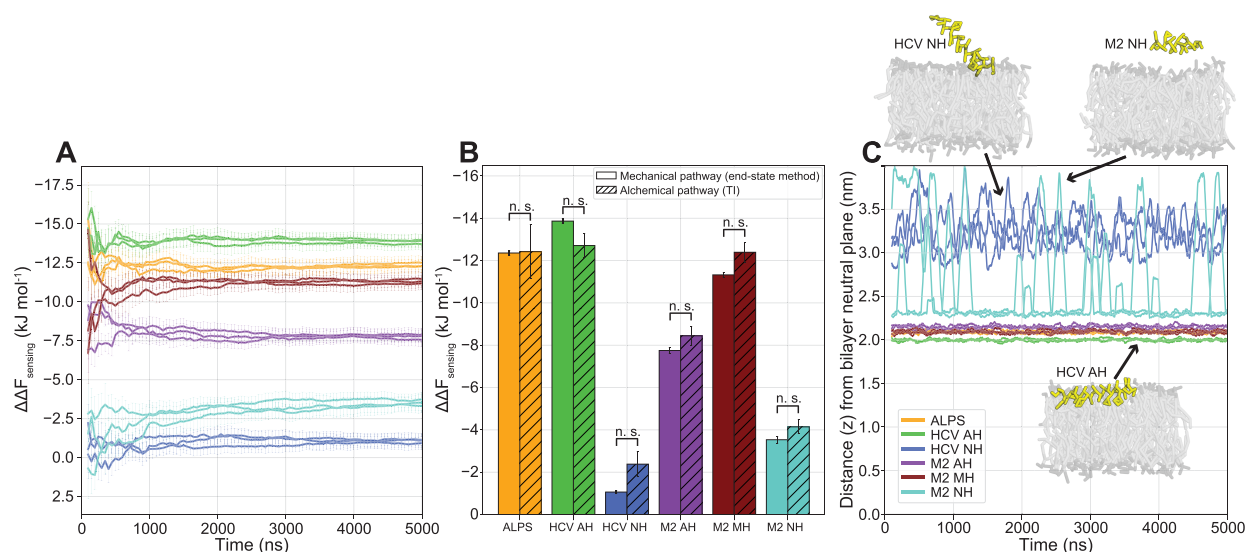
Figure 4. (A) Cumulative moving average of $\Delta\Delta F_{sensing}$ for triplicate 5 μs runs. (B) Comparison between our mechanical end-state method (averages and standard deviations of the three 5 μs runs in A) and free energy calculation via the alchemical pathway (TI). P values were calculated with the two-tailed Welch's t test, which showed no statistically significant differences for any of the peptides ($p > 0.05$). (C) Distance (z) between the peptide and the bilayer neutral plane (100 ns moving average) for the tensionless runs in A. Absolute values are taken to account for periodic boundary crossings. Insets show typical conformations for HCV AH (fully membrane bound), HCV NH (partly membrane bound), and M2 NH (fully unbound).

viruses, including Zika, Dengue, and West Nile viruses.[41] Just like the original work, we will also include the negative control HCV NH, where three-point mutations nullify the amphipathicity of the peptide, resulting in a loss of antiviral activity.[39] Finally, and along the same lines, we will consider an AH derived from the M2 protein of the influenza virus that showed antiviral activity against four different influenza strains.[42] A variant with increased amphipathicity (named M2 MH) showed an 16.4-fold increase in anti-influenza inhibitory effect. In contrast, the potency is abolished for a variant with low amphipathicity (named M2 NH), which we will use as a second negative control.

For simplicity, we opted to perform all simulations with pure zwitterionic POPC model membranes. However, we emphasize that our method is in no way restricted to membrane composition and that it could therefore be utilized to additionally study the effect of lipid membrane composition on lipid packing defect sensing.

3.1. Calculating Sensing Free Energies via the Mechanical Pathway. We performed CGMD simulations of these peptides adhered to the surface of membranes at equilibrium (0% relative strain) and at increasing degrees of stretching (up to 16.5% relative strain) and measured the resulting change in surface tension $\sigma(A)$ (Figure 3B). Consistent with eq 4, we observed near-linear behavior for small strains both with and without peptides present. It becomes clear that peptides binding to the surface of a membrane reduce the surface tension imposed by the fixed boundary conditions to keep the system at a constant area. In other words, the adhered peptides reduce the work of stretching. Also, we can already observe that the inactive peptides HCV NH and M2 NH cause a much smaller reduction in this tension than the active curvature sensors. Now, we can calculate the free energy of sensing ($\Delta\Delta F_{sensing}$) by integrating over these curves (eq 7), i.e., we calculate the area enclosed by the "no peptide" curve ($\sigma(A)$; black line in

Figure 3B) and the curve for the peptide of interest ($\sigma'(A)$; colored line). Since the tension reduction is approximately constant for different membrane areas, taking this integral over all 6 points (dotted line in Figure 3C) or only the end states (0% and 16.5% relative strain; solid line in Figure 3C) yields the same result, at least within the measurement error. Thus, only two simulations at the extremes suffice to accurately calculate $\Delta\Delta F_{sensing}$. We note that this $\Delta\Delta F_{sensing}$ is calculated from simulations at constant area. With additional simulations at constant tension (see SI), we show that the resulting correction terms that arise from transitioning from constant area to constant tension ensembles are negligible. Therefore, we proceeded to use the end-state mechanical calculations at constant area for all of the following results described in this paper.

3.2. "CHAOS" Parameter: An End-State-Invariant Measure for Lipid Packing Sensing Ability. We note that one can only interpret the $\Delta\Delta F_{sensing}$ relative between different peptides, since the absolute values depend on the (arbitrary) choice of the two end states (Figure 3C). We chose end states with a large difference in tension since this inflates the value of $\Delta\Delta F_{sensing}$ and therefore enhances the reliability of peptide ranking, i.e., the relative differences in $\Delta\Delta F_{sensing}$ overcome the sampling error. In fact, because of a linear relationship between the free energy and the tension (eq 6), we can define an end-state-invariant property that we coin the "characteristic area of sensing" (aptly abbreviated to CHAOS) since it has the dimension of area per molecule. This CHAOS parameter is the relative difference in binding free energy (= sensing) normalized by the difference in surface tension between the peptide-free reference systems

$$\text{CHAOS} = \frac{\Delta\Delta F_{sensing}}{\Delta\sigma(A)} = \frac{\Delta\Delta F_{sensing}}{\sigma(A_0) - \sigma(A)} \qquad (8)$$

The surface tension of the peptide-free reference systems is chosen pragmatically because of the smaller sampling error in
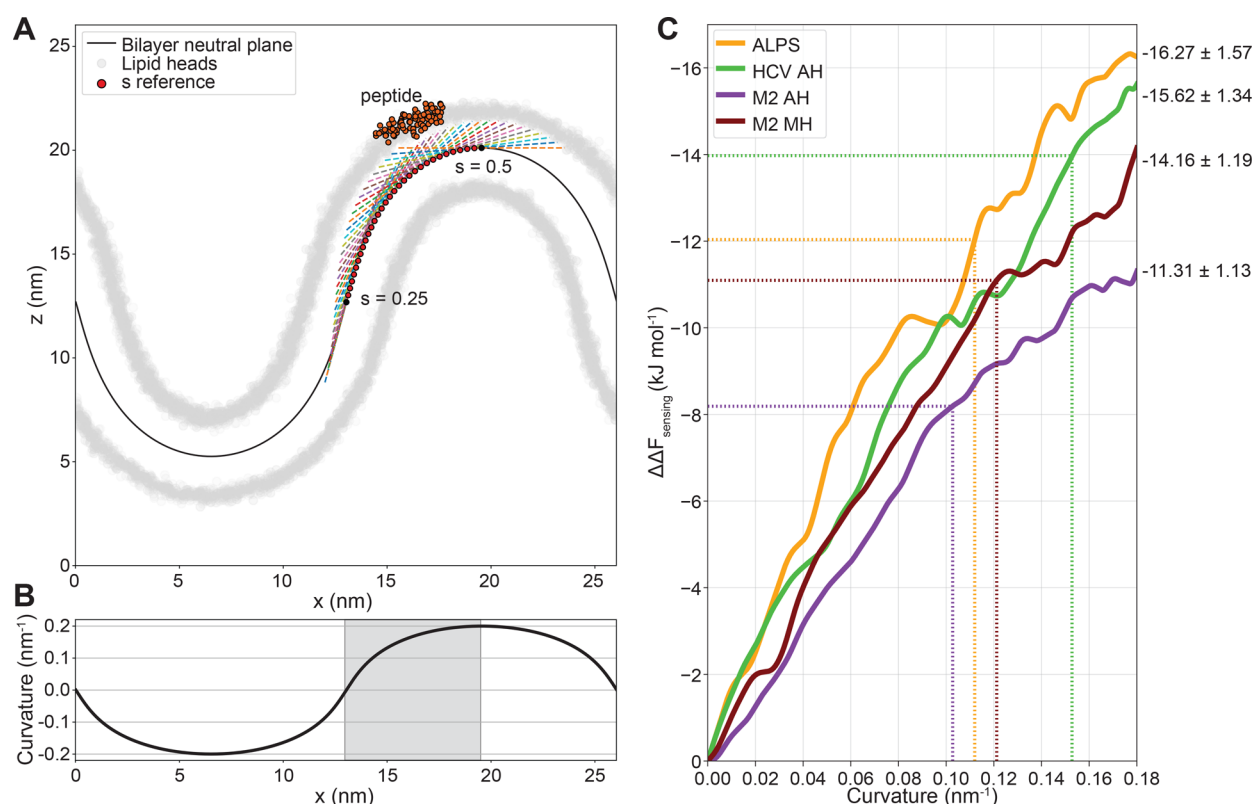
Figure 5. (A) Setup for umbrella sampling of the peptide−membrane interaction along a buckled membrane. Umbrella potential acts along the tangent (dashed lines) at select reference points (s). (B) Curvature of the buckled bilayer neutral plane as a function of the x coordinate. Gray area indicates the sampled region. (C) Sensing free energy as a function of curvature along the buckled membrane. Dotted lines indicate the free energy values calculated from the end-state mechanical method (Figure 3C) and their corresponding curvatures.

pure lipid membrane systems. In the constant tension ensemble, both systems in fact converge to the same surface tension, which yields similar magnitudes of the CHAOS parameter (see SI). Indeed, when we plot the CHAOS parameter against the range of $\Delta\sigma$'s simulated, we observe an approximately constant CHAOS value for every peptide (Figure 3D). The ranking and relative distances between these values for the different peptides remains fully consistent with the $\Delta\Delta F_{sensing}$ values, yet they are independent of the choice of end states.

The CHAOS parameter can be, in part, interpreted as the area increase upon adhesion of a given peptide to a tensionless membrane within the corresponding NpT ensemble (see Table SI2). However, its magnitude will always be slightly bigger since it is additionally determined by the peptide's ability to soften the membrane, i.e., lowering the area compressibilty K_A and thereby reducing the mechanical work of stretching. In fact, CHAOS is a striking abbreviation since its magnitude directly reflects the ability of the peptide to disorder the packing of lipid tails via creation of excess leaflet area (tension). As per this definition, we speculate that CHAOS parameters may be directly comparable to experimental values obtained from liposome binding assays[44] and Langmuir−Blodgett experiments in which the surface tension of a lipid monolayer at the air−water interface can be measured upon adhesion of surfactants (e.g., amphipathic peptides).[45]

3.3. Convergence, Reproducibility, and Comparison to Conventional Alchemical Pathways. We performed three independent reruns of 5 μs per simulation to assess the reproducibility and convergence of our method (Figure 4A).

This showed that after approximately 1 μs, the calculated free energies of the independent runs converged to the same value (within the margin of error).

Consistent with thermodynamic theory (eq 3, Figure 2A), the sensing free energies calculated via the mechanical pathway between the end states closely match the free energies calculated by TI (Figure 4B, Figure SI2), with no statistically significant differences between the two methods for all of the peptides tested. We stress that while producing the same results, there is a significant computational speed-up for our mechanical end-state method compared to TI. Free energy calculation via the mechanical pathway can be done reliably in 2 μs of simulation (1 μs for each of the two states), whereas TI required 74 μs. This 37× speed-up is indispensable when considering high-throughput calculation of the membrane binding properties of peptides.

In line with the experimental results and the original design principles, the peptides with mutated hydrophobic faces (HCV NH and M2 NH) indeed have a compromised sensing ability compared to the original peptides that were derived from HCV AH and M2 AH, respectively (see Figure 4B). This reduced sensing free energy is mainly due to (partial) detachment from the membrane during our MD simulations (Figure 4C), which renders them incapable of reducing the membrane surface tension.

3.4. Transferability between Tension Sensing and Curvature Sensing. To evaluate the transferability between lipid packing defect sensing in a flat membrane (tension in both leaflets) and positive curvature (tension in the outer, compression in the inner leaflet), we performed umbrella
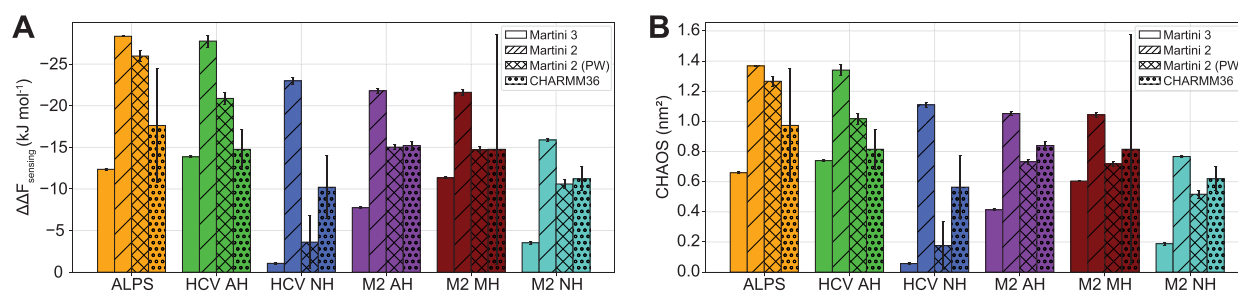
Figure 6. Comparison of lipid packing sensing of peptides with the Martini 3 (version 3.0.0), Martini 2 (version 2.2), Martini 2 with polarizable water (PW, version 2.3P), and atomistic CHARMM36 force fields in terms of sensing free energy (A) and CHAOS parameter (B). Reported values and error bars are averages and standard deviations of three independent replicas. Martini 3 data is the same as that in Figure 4. Martini 2 and atomistic runs were 1 μs each.

sampling (US) along a buckled POPC membrane (Figure 5A and 5B) as described previously.[12] The poorly binding HCV NH and M2 NH peptides were not considered here since good surface adhesion is a prerequisite in this approach. From this experiment, we obtained sensing free energy profiles as a function of membrane curvature (Figure 5C) that we can directly compare with the free energy values we obtained through our end-state mechanical method (Figure 3C). We find that US along the membrane buckle yields a similar ranking as our end-state free energy calculation method with flat membranes, with the exception that ALPS outperforms HCV AH by 0.65 kJ mol^{-1} on the buckle (Figure 5C). However, considering the large error in the US method (95% confidence intervals = 1.57 and 1.34 kJ mol^{-1}, respectively), we do not consider this difference to be significant. Thus, the ability of an α-helical peptide to sense leaflet curvature is indeed directly relatable to its ability to sense lipid packing defects in a flat membrane.

Furthermore, we can use this membrane buckle to check whether the degree of stretching we use in our end-state method realistically represents the membrane curvature that it should resemble ($1/R \approx 1/12.5 = 0.08$ nm^{-1}, see derivation in SI). We do this by matching the $\Delta\Delta F_{sensing}$ values we obtained from our end-state method with the free energy profiles from US over the buckled membrane (Figure 5C), which yields curvatures ranging from 0.11 to 0.16 nm^{-1} (dotted lines in Figure 5C). Since the buckled membrane has a cylindrical geometry (only curved in one dimension), the mean curvatures of a corresponding vesicle (curved in two dimensions) should be reduced by a factor two: from 0.055 to 0.080 nm^{-1}. This results in a range of vesicle radii of approximately 12.5−18 nm, which is in line with the estimated vesicle sizes in the tensed membrane systems based on leaflet strain elastic theory as derived in the SI.

3.5. Comparing Lipid Force Fields on Sensing Free Energy and CHAOS Parameters.
A major goal in the parametrization of atomistic and CG lipid force fields is to reproduce the partitioning free energies of biomolecules between polar (solvent) and apolar (lipid membrane) phases. Recently, it was shown that the new Martini 3 model is able to correctly characterize the general binding behavior of membrane peripheral proteins.[46] In addition, we now have a unique tool in hand to quantitatively compare force fields on their ability to reproduce the thermodynamic properties associated with membrane peripheral protein binding such as relative binding free energies (lipid packing sensing) and the concomitant CHAOS parameter. Here, we perform such a

comparison for Martini 3, Martini 2 (version 2.2[7,47] and version 2.3P with polarizable water (PW)[48] and PME electrostatics), and the atomistic CHARMM36 force field (Figure 6A and 6B). For the six peptides we study throughout this paper, we find that the new Martini 3 model qualitatively reproduces the general trends derived from experimental studies: HCV AH outperforms the inactivated mutant HCV NH,[39] and M2 MH is more potent than M2 AH, while the activity is indeed strongly reduced for M2 NH.[42]

In contrast, these trends are not captured correctly by the Martini 2 model, which severely overestimates $\Delta\Delta F_{sensing}$ and CHAOS values compared to the other force fields. This is caused by exaggerated peptide−membrane binding (i.e., the peptides are "too hydrophobic"), as confirmed by the density plots and insertions depths (see Figure SI3 and Table SI3). We find that this behavior is improved when using Martini 2 with PW, especially for peptides with net charge (HCV NH, M2 AH, M2 MH, and M2 NH), for which it more closely matches the values we obtained with Martini 3 and CHARMM36.

The $\Delta\Delta F_{sensing}$ and CHAOS values calculated from atomistic simulations with CHARMM36 are within the same range as the Martini 3 and Martini 2 (with PW) results. However, we note that measurement errors are considerably larger because of the slower convergence compared to the CG force fields, rendering sufficient sampling of (un)binding and peptide refolding events challenging in practice despite the high computational efficiency of our method. This was especially true for M2 MH, which displayed strong membrane binding in one replica and weak binding or even partial detachment in the other two, resulting in a large measurement error (see Figure SI3 and Table SI3).

Finally, we examined the membrane insertion depths of the peptides in the different force fields and found that this insertion is markedly shallower in Martini 3 than that in CHARMM36, i.e., peptides in Martini 3 behave "too hydrophilic" (see Figure SI3 and Table SI3) despite qualitatively reproducing the experimental trends. Part of this discrepancy could be related to the structural plasticity of peptides in the atomistic simulation, which makes a direct comparison to CG simulations less straightforward. Nevertheless, the observed systematic and marked reduction in peptide insertion depths along with an often lower CHAOS parameter suggests that Martini 3 may have a tendency to underestimate the membrane binding behavior of proteins with respect to CHARMM36 even though overall relative binding free energies seem improved with respect to the previous Martini versions. One of the main founding principles
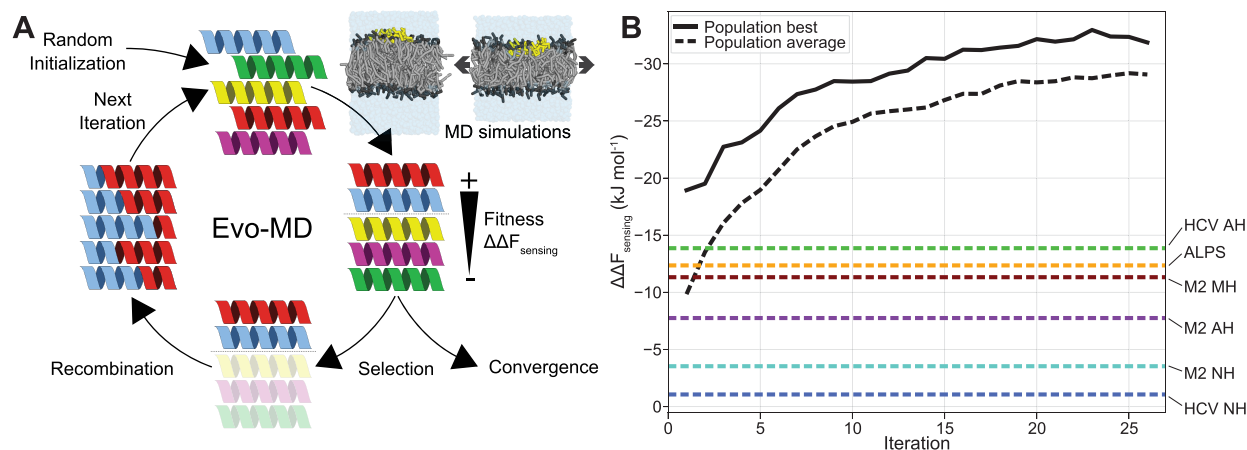
Figure 7. (A) Schematic representation of the basic concept of evolutionary molecular dynamics (Evo-MD). Adapted from 49. Generated peptides (starting from a population of random sequences) are iteratively ranked on their "fitness" ($\Delta\Delta F_{sensing}$), as determined by the end-state mechanical pathway method described in this paper. Best sequences are picked and recombined to produce the next generation, leading to gradual evolution toward the optimal lipid packing sensing peptides. (B) Within 25 iterations of Evo-MD, we observe convergence at a $\Delta\Delta F_{sensing}$ that far exceeds the values we see for current state-of-the-art lipid packing defect sensors (e.g., HCV AH, ALPS, and M2 MH).

of the original Martini model was to reproduce partitioning free energies of fluid mixtures by reproducing density profiles, and which determine the insertion depths of molecules. It is thus somewhat surprising that the membrane insertion depth of the proteins are in fact less well reproduced in Martini 3 than in the older versions.

3.6. Using "CHAOS Control" To Improve Force Field Development. In this work, we selected six peptides based on the fact that they are of biological/pharmaceutical importance and experimentally well characterized. However, the similarity in their CHAOS parameters suggests that peptides can have overlapping physicochemical properties despite having very different sequences. This raises the question of whether a physicochemically more diverse set of peptides can be constructed that more efficiently and strategically enables both the benchmarking and the parametrization of force fields.

We recently proposed a physics-based inverse design approach coined evolutionary molecular dynamics (Evo-MD).[49] Evo-MD relies on the principle that (large) experimental data contributes to solving biophysical problems independently via the parametrization of bottom-up CG force fields. Evo-MD features a directed evolution (genetic algorithm) of peptide sequences that starts with a set ("population") of completely random peptide sequences ("individuals") and computes the corresponding "fitness" value for every sequence from one or more MD simulations. Then, in each generation/iteration, analogous to Darwin's "reproduction of the fittest", the best scoring individuals are recombined and consequently produce offspring that resemble their predecessors but are slightly different due to both random crossovers and infrequent point mutations. By repeating this cycle (Figure 7A) for several iterations, the fitness of the best individuals in the population should improve until it converges to an optimum value. We previously demonstrated the utility of this concept by resolving the optimal cholesterol sensing transmembrane domain.[49]

With the highly efficient mechanical pathway method we present here, we can now perform a similar optimization for the lipid packing defect sensing problem, which would be unfeasible with previous methods, like TI, because of their computational expense. Figure 7B illustrates the utility of Evo-MD in generating peptide sequences (with a fixed length of 24 amino acids) with highly diverse sensing free energies. We emphasize that, in the current work, these results solely serve as a proof of principle and that details on the sequences of the resolved optima as well as their experimental validation will be published in a separate upcoming paper.

An important and fundamental question is whether the natural and nature-derived peptides that we studied in this work are optimal for lipid packing defect sensing. Intriguingly, the evolutionary convergence in Figure 7B suggests that known curvature sensors in nature (like ALPS and HCV AH) are in fact far from optimal. A general feature among the optimized sequences ($\Delta\Delta F_{sensing}$ < −30 kJ mol⁻¹, see Figure 7B) is a strong enrichment in big aromatic residues (F and W) to maximize membrane insertion depth, peptide volume, and consequent tension generation. This shows that our method successfully finds and amplifies a well-known mechanistic feature (W/F insertion) that underlies lipid packing defect sensing by natural peptides.[32,37] We argue that the many evolutionary constraints imposed by nature's complexity (e.g., solubility, protein−protein interactions, trafficking, and many more) likely hinder the optimization of a single objective. This argument is in full agreement with the notion that curvature sensing in nature is a subtle balance between general membrane binding and specific curvature recognition.[34] In addition, our results suggest that—since defect sensing also implies the active induction of leaflet strain—curvature sensors should conserve the structural integrity of the lipid membranes they adhere to. Consequently, the global optimum of a desired single objective such as defect or curvature sensing in our example may thus lie far outside the applicability domain of data-science-based generative peptide models, i.e., generative models trained on large data sets of native sequences, because the training data is too distinct from the theoretical optima.

We argue that directed evolution approaches such as Evo-MD may offer a valuable benchmark platform for lipid force fields. First, the primary aim of force fields is to reproduce physicochemical driving forces—trends rather than absolutes—and therefore force fields must at least reproduce the global physicochemical features of the optimized sequences. Second, Evo-MD yields sequences over the whole range in

relative binding free energy by gradually maximizing the relevant chemical distinction between the peptides in a well-spaced manner.

Of course, a main limitation of this approach is that CG models such as Martini do not predict secondary and tertiary structures. As most amphipathic peptides fold into an α-helix upon binding to the membrane surface, we used fixed helical folding throughout our CG models. To test the influence of this enforced helicity, we performed additional simulations with peptides modeled as random coils and found that the way in which folding affects the CHAOS value strongly differs per peptide (see SI). We observe that highly scoring peptides (ALPS, HCV AH, M2 AH, M2 MH, and also the optima resolved by Evo-MD) lose some activity when remodeled as a random coil, although never dropping below a baseline CHAOS value of ~0.4 nm^2. Conversely, we find that the sensing ability of poorly binding peptides (like HCV NH) could improve when adopting a fully coiled conformation. Taken together, we argue that optimization of sensing is most dominantly determined by the peptide's general amino acid composition (i.e., its overall hydrophobicity) and only in the second instance by peptide structure. This is in line with similar findings in the context of membrane-binding antimicrobial peptides,[50] although it is important to note that helical folding in many cases facilitates the optimal positioning of residues into polar and apolar faces, as exemplified by the amphipathic peptides studied here. These findings imply that one can effectively generate sequences with high CHAOS values and subsequently resolve the structure via atomistic simulations or—if the goal is direct comparison—restrain the structure in both the atomistic and the CG simulations to, for example, an α-helix. In addition, the Evo-MD runs can be performed in conjunction with "on the fly" structure prediction without severe loss of computational efficiency, since the MD simulation will remain the rate-limiting step.

4. CONCLUSIONS

We found that a peptide's ability to sense lipid packing defects in biological membranes can be redefined as the peptide's ability to reduce membrane tension in a leaflet under excess strain or, equivalently, the peptide's ability to reduce the mechanical work required to stretch the membrane (leaflet). We demonstrated that calculation of such a reduction in mechanical work offers a highly efficient and accurate route for the estimation of relative membrane binding free energies. This resulting quantification of lipid packing sensing ability by the membrane peripheral protein can be expressed as the sensing free energy ($\Delta\Delta F_{\text{sensing}}$) or the here-defined characteristic area of sensing (CHAOS) parameter, which is independent of the choice of end states. The method only requires knowledge of the individual pressure components over the course of the simulation trajectory to calculate the system's surface tension, a quantity which virtually all molecular dynamics packages provide.

We used this novel end-state method to compare the performance of the new Martini 3 coarse-grained force field with the previous Martini 2 for biorelevant lipid packing defect sensing peptides. We observed that Martini 3 most accurately reproduced the experimental trends, although the relative binding free energies were generally lower than those calculated from atomistic simulations. In contrast, Martini 2 severely overestimated peptide–membrane interactions and

consequent packing defect sensing. Finally, since defect sensing implies both easing and active induction of leaflet strain, we hypothesize that lipid packing defect and curvature sensors in nature must be far from optimal since these proteins must largely conserve the structural integrity of the lipid membranes they adhere to. We argue that the extrema, i.e., the optimal sequences, particularly provide valuable benchmarks for force field development and comparison because their distinct physicochemical signatures directly reflect how a force field captures the physicochemical mechanisms of sensing.

■ ASSOCIATED CONTENT

Ⓢ Supporting Information

The Supporting Information is available free of charge at https://pubs.acs.org/doi/10.1021/acs.jctc.2c00222.

> Derivation of the relation between relative strain and vesicle diameter; peptide sequences and properties; relation between sensing free energies in constant area and constant tension ensembles; CHAOS parameters compared to the area increase upon peptide adhesion; $\partial V/\partial\lambda$ profiles for thermodynamic integration; density plots of peptide−membrane binding in different force fields; insertion depths of peptide−membrane binding in different force fields; effect of HCV AH tertiary structure on CHAOS parameter (PDF)

■ AUTHOR INFORMATION

Corresponding Author

Herre Jelger Risselada − *Leiden Institute of Chemistry, Leiden University, Leiden 2300 RA, The Netherlands; Department of Physics, Technical University Dortmund, Dortmund 44221, Germany; Institute for Theoretical Physics, Georg-August-University Göttingen, Göttingen 37077, Germany;* ⓞ orcid.org/0000-0003-1410-6570; Email: jelger.risselada@tu-dortmund.de

Authors

Niek van Hilten − *Leiden Institute of Chemistry, Leiden University, Leiden 2300 RA, The Netherlands;* ⓞ orcid.org/0000-0003-1204-2489

Kai Steffen Stroh − *Department of Physics, Technical University Dortmund, Dortmund 44221, Germany; Institute for Theoretical Physics, Georg-August-University Göttingen, Göttingen 37077, Germany;* ⓞ orcid.org/0000-0001-5239-7124

Complete contact information is available at: https://pubs.acs.org/10.1021/acs.jctc.2c00222

Notes

The authors declare no competing financial interest.

■ ACKNOWLEDGMENTS

■ REFERENCES

(1) Hatzakis, N. S; Bhatia, V. K; Larsen, J.; Madsen, K. L; Bolinger, P.-Y.; Kunding, A. H; Castillo, J.; Gether, U.; Hedegard, P.; Stamou, D. How curved membranes recruit amphipathic helices and protein anchoring motifs. *Nat. Chem. Biol.* **2009**, *5*, 835−841.

(2) Bhatia, V. K.; Hatzakis, N. S.; Stamou, D. A unifying mechanism accounts for sensing of membrane curvature by BAR domains, amphipathic helices and membrane-anchored proteins. *Semin. Cell Dev. Biol.* **2010**, *21*, 381−390.

(3) Ouberai, M. M.; Wang, J.; Swann, M. J.; Galvagnion, C.; Guilliams, T.; Dobson, C. M.; Welland, M. E. α-Synuclein Senses Lipid Packing Defects and Induces Lateral Expansion of Lipids Leading to Membrane Remodeling. *J. Biol. Chem.* **2013**, *288*, 20883−20895.

(4) Kim, S.; Oh, M. I.; Swanson, J. M. J. Stressed Lipid Droplets: How Neutral Lipids Relieve Surface Tension and Membrane Expansion Drives Protein Association. *J. Phys. Chem. B* **2021**, *125*, 5572−5586.

(5) Giménez-Andrés, M.; Čopič, A.; Antonny, B. The Many Faces of Amphipathic Helices. *Biomolecules* **2018**, *8*, 45.

(6) Nepal, B.; Leveritt, J.; Lazaridis, T. Membrane Curvature Sensing by Amphipathic Helices: Insights from Implicit Membrane Modeling. *Biophys. J.* **2018**, *114*, 2128−2141.

(7) Marrink, S. J.; Risselada, H. J.; Yefimov, S.; Tieleman, D. P.; de Vries, A. H. The MARTINI Force Field: Coarse Grained Model for Biomolecular Simulations. *J. Phys. Chem. B* **2007**, *111*, 7812−7824.

(8) Souza, P. C. T.; Alessandri, R.; Barnoud, J.; Thallmair, S.; Faustino, I.; Grünewald, F.; Patmanidis, I.; Abdizadeh, H.; Bruininks, B. M. H.; Wassenaar, T. A.; Kroon, P. C.; Melcr, J.; Nieto, V.; Corradi, V.; Khan, H. M.; Domański, J.; Javanainen, M.; Martinez-Seara, H.; Reuter, N.; Best, R. B.; Vattulainen, I.; Monticelli, L.; Periole, X.; Tieleman, D. P.; de Vries, A. H.; Marrink, S. J. Martini 3: a general purpose force field for coarse-grained molecular dynamics. *Nat. Methods* **2021**, *18*, 382−388.

(9) Kirkwood, J. G. Statistical Mechanics of Fluid Mixtures. *J. Chem. Phys.* **1935**, *3*, 300−313.

(10) Bennett, C. H. Efficient estimation of free energy differences from Monte Carlo data. *J. Comput. Phys.* **1976**, *22*, 245−268.

(11) Jackman, J. A. Antiviral peptide engineering for targeting membrane-enveloped viruses: Recent progress and future directions. *Biochim. Biophys. Acta Biomembr.* **2022**, *1864* (2), 183821.

(12) Stroh, K. S.; Risselada, H. J. Quantifying Membrane Curvature Sensing of Peripheral Proteins by Simulated Buckling and Umbrella Sampling. *J. Chem. Theory Comput.* **2021**, *17*, 5276−5286.

(13) van Hilten, N.; Stroh, K. S.; Risselada, H. J. Membrane Thinning Induces Sorting of Lipids and the Amphipathic Lipid Packing Sensor (ALPS) Protein Motif. *Front. Physiol.* **2020**, *11*, 250.

(14) Gautier, R.; Bacle, A.; Tiberti, M. L.; Fuchs, P. F.; Vanni, S.; Antonny, B. PackMem: A Versatile Tool to Compute and Visualize Interfacial Packing Defects in Lipid Bilayers. *Biophys. J.* **2018**, *115*, 436−444.

(15) Lipowsky, R. Coupling of bending and stretching deformations in vesicle membranes. *Adv. Colloid Interface Sci.* **2014**, *208*, 14−24. Special issue in honor of Wolfgang Helfrich.

(16) Wassenaar, T. A.; Ingólfsson, H. I.; Bóckmann, R. A.; Tieleman, D. P.; Marrink, S. J. Computational Lipidomics with insane: A Versatile Tool for Generating Custom Membranes for Molecular Simulations. *J. Chem. Theory Comput.* **2015**, *11*, 2144−2155.

(17) Tien, M. Z.; Sydykova, D. K.; Meyer, A. G.; Wilke, C. O. PeptideBuilder: A simple Python library to generate model peptides. *PeerJ* **2013**, *1*, e80.

(18) Kroon, P. C. Aggregate, Assemble, Automate. Ph.D. Thesis, University of Groningen, 2020.

(19) Berendsen, H. J. C.; Postma, J. P. M.; van Gunsteren, W. F.; Di Nola, A.; Haak, J. R. Molecular Dynamics with Coupling to an External Bath. *J. Chem. Phys.* **1984**, *81*, 3684−3690.

(20) Parrinello, M.; Rahman, A. Polymorphic transitions in single crystals: A new molecular dynamics method. *J. Appl. Phys.* **1981**, *52*, 7182−7190.

(21) Jorgensen, W. L.; Chandrasekhar, J.; Madura, J. D.; Impey, R. W.; Klein, M. L. Comparison of simple potential functions for simulating liquid water. *J. Chem. Phys.* **1983**, *79*, 926−935.

(22) Huang, J.; MacKerell, A. D. CHARMM36 all-atom additive protein force field: Validation based on comparison to NMR data. *J. Comput. Chem.* **2013**, *34*, 2135−2145.

(23) Lee, J.; Cheng, X.; Swails, J. M.; Yeom, M. S.; Eastman, P. K.; Lemkul, J. A.; Wei, S.; Buckner, J.; Jeong, J. C.; Qi, Y.; Jo, S.; Pande, V. S.; Case, D. A.; Brooks, C. L.; MacKerell, A. D.; Klauda, J. B.; Im, W. CHARMM-GUI Input Generator for NAMD, GROMACS, AMBER, OpenMM, and CHARMM/OpenMM Simulations Using the CHARMM36 Additive Force Field. *J. Chem. Theory Comput.* **2016**, *12*, 405−413.

(24) Abraham, M. J.; Murtola, T.; Schulz, R.; Páll, S.; Smith, J. C.; Hess, B.; Lindahl, E. GROMACS: High Performance Molecular Simulations Through Multi-Level Parallelism from Laptops to Supercomputers. *Software X* **2015**, *1−2*, 19−25.

(25) Bussi, G.; Donadio, D.; Parrinello, M. Canonical Sampling Through Velocity Rescaling. *J. Chem. Phys.* **2007**, *126*, 014101.

(26) Grubmüller, H.; Heller, H.; Windemuth, A.; Schulten, K. Generalized Verlet Algorithm for Efficient Molecular Dynamics Simulations with Long-range Interactions. *Mol. Simul.* **1991**, *6*, 121−142.

(27) van Gunsteren, W. F.; Berendsen, H. J. C.; Rullmann, J. A. C. Inclusion of reaction fields in molecular dynamics. Application to liquid water. *Faraday Discuss. Chem. Soc.* **1978**, *66*, 58.

(28) Huang, J.; Rauscher, S.; Nawrocki, G.; Ran, T.; Feig, M.; de Groot, B. L.; Grubmüller, H.; MacKerell, A. D. CHARMM36m: an improved force field for folded and intrinsically disordered proteins. *Nat. Methods* **2017**, *14*, 71−73.

(29) Darden, T.; York, D.; Pedersen, L. Particle mesh Ewald: AnN·log(N) method for Ewald sums in large systems. *J. Chem. Phys.* **1993**, *98*, 10089−10092.

(30) Hess, B.; Bekker, H.; Berendsen, H. J. C.; Fraaije, J. G. E. M. LINCS: A linear constraint solver for molecular simulations. *J. Comput. Chem.* **1997**, *18*, 1463−1472.

(31) Bigay, J.; Casella, J. F.; Drin, G.; Mesmin, B.; Antonny, B. ArfGAP1 responds to membrane curvature through the folding of a lipid packing sensor motif. *EMBO J.* **2005**, *24*, 2244−2253.

(32) Drin, G.; Casella, J. F.; Gautier, R.; Boehmer, T.; Schwartz, T. U.; Antonny, B. A general amphipathic alpha-helical motif for sensing membrane curvature. *Nat. Struct. Mol. Biol.* **2007**, *14*, 138−146.

(33) Cabrera, M.; Langemeyer, L.; Mari, M.; Rethmeier, R.; Orban, I.; Perz, A.; Bröcker, C.; Griffith, J.; Klose, D.; Steinhoff, H.-J.; Reggiori, F.; Engelbrecht-Vandré, S.; Ungermann, C. Phosphorylation of a membrane curvature−sensing motif switches function of the HOPS subunit Vps41 in membrane tethering. *J. Cell Biol.* **2010**, *191*, 845−859.

(34) Antonny, B. Mechanisms of membrane curvature sensing. *Annu. Rev. Biochem.* **2011**, *80*, 101−123.

(35) Reynaud, A.; Magdeleine, M.; Patel, A.; Gay, A. S.; Debayle, D.; Abelanet, S.; Antonny, B. Tumor protein D54 binds intracellular nanovesicles via an amphipathic lipid packing sensor (ALPS) motif. *bioRxiv* **2021** DOI: 10.1101/2021.12.03.471088.

(36) Gonzalez-Rubio, P.; Gautier, R.; Etchebest, C.; Fuchs, P. F.J. Amphipathic-Lipid-Packing-Sensor interactions with lipids assessed by atomistic molecular dynamics. *Biochim. Biophys. Acta Biomembr.* **2011**, *1808*, 2119−2127.

(37) Vanni, S.; Vamparys, L.; Gautier, R.; Drin, G.; Etchebest, C.; Fuchs, P. F.; Antonny, B. Amphipathic lipid packing sensor motifs: probing bilayer defects with hydrophobic residues. *Biophys. J.* **2013**, *104*, 575−584.

(38) Vanni, S.; Hirose, H.; Barelli, H.; Antonny, B.; Gautier, R. A sub-nanometre view of how membrane curvature and composition modulate lipid packing and protein recruitment. *Nat. Commun.* **2014**, *5*, 4916.

(39) Cho, N.-J.; Dvory-Sobol, H.; Xiong, A.; Cho, S.-J.; Frank, C. W.; Glenn, J. S. Mechanism of an Amphipathic α-Helical Peptide's Antiviral Activity Involves Size-Dependent Virus Particle Lysis. *ACS. Chem. Biol.* **2009**, *4*, 1061−1067.

(40) Jackman, J. A.; Zan, G. H.; Zhdanov, V. P.; Cho, N.-J. Rupture of Lipid Vesicles by a Broad-Spectrum Antiviral Peptide: Influence of Vesicle Size. *J. Phys. Chem. B* **2013**, *117*, 16117−16128.

(41) Jackman, J. A.; Costa, V. V.; Park, S.; Real, A. L. C. V.; Park, J. H.; Cardozo, P. L.; Ferhan, A. R.; Olmo, I. G.; Moreira, T. P.; Bambirra, J. L.; Queiroz, V. F.; Queiroz-Junior, C. M.; Foureaux, G.; Souza, D. G.; Ribeiro, F. M.; Yoon, B. K.; Wynendaele, E.; De Spiegeleer, B.; Teixeira, M. M.; Cho, N.-J. Therapeutic treatment of Zika virus infection using a brain-penetrating antiviral peptide. *Nat. Mater.* **2018**, *17*, 971−977.

(42) Jung, Y.; Kong, B.; Moon, S.; Yu, S.-H.; Chung, J.; Ban, C.; Chung, W.-J.; Kim, S.-G.; Kweon, D.-H. Envelope-deforming antiviral peptide derived from influenza virus M2 protein. *Biochem. Biophys. Res. Commun.* **2019**, *517*, 507−512.

(43) Gautier, R.; Douguet, D.; Antonny, B.; Drin, G. HELIQUEST: a web server to screen sequences with specific α-helical properties. *Bioinformatics* **2008**, *24*, 2101−2102.

(44) Jensen, M. B.; Bhatia, V. K.; Jao, C. C.; Rasmussen, J. E.; Pedersen, S. L.; Jensen, K. J.; Langen, R.; Stamou, D. Membrane Curvature Sensing by Amphipathic Helices: A Single Liposome Study Using α-synuclein and Annexin B12. *J. Biol. Chem.* **2011**, *286*, 42603−42614.

(45) Rabe, M.; Schwieger, C.; Zope, H. R.; Versluis, F.; Kros, A. Membrane Interactions of Fusogenic Coiled-Coil Peptides: Implications for Lipopeptide Mediated Vesicle Fusion. *Langmuir* **2014**, *30*, 7724−7735.

(46) Srinivasan, S.; Zoni, V.; Vanni, S. Estimating the accuracy of the MARTINI model towards the investigation of peripheral protein-membrane interactions. *Faraday Discuss.* **2021**, *232*, 131−148.

(47) Monticelli, L.; Kandasamy, S. K.; Periole, X.; Larson, R. G.; Tieleman, D. P.; Marrink, S.-J. The MARTINI Coarse-Grained Force Field: Extension to Proteins. *J. Chem. Theory Comput.* **2008**, *4*, 819−834.

(48) Yesylevskyy, S. O.; Schäfer, L. V.; Sengupta, D.; Marrink, S. J. Polarizable Water Model for the Coarse-Grained MARTINI Force Field. *PLoS Comput. Biol.* **2010**, *6*, e1000810.

(49) Methorst, J.; van Hilten, N.; Risselada, H. J. Inverse design of cholesterol attracting transmembrane helices reveals a paradoxical role of hydrophobic length. *bioRxiv* **2021** DOI: 10.1101/2021.07.01.450699.

(50) Wimley, W. C. Describing the Mechanism of Antimicrobial Peptide Action with the Interfacial Activity Model. *ACS. Chem. Biol.* **2010**, *5*, 905−917.